

Generalized Theory of BOC Signal Unambiguous Tracking With Two-Dimensional Loops

ZHENG YAO^{ID}, Member, IEEE
Tsinghua University, Beijing, China

YANG GAO
Beijing Satellite Navigation Center, Beijing, China

YANG GAO
MINGQUAN LU
Tsinghua University, Beijing, China

The multipeaked correlation functions of binary offset carrier (BOC) modulated signals introduce an ambiguity threat into the code tracking. Several techniques have been proposed to solve this problem, such as a class of two-dimensional (2-D) tracking techniques, in which the spreading code and the subcarrier are tracked separately. In this paper, the key properties of correlation functions and the theoretical tracking performance analysis considering noise and multipath environments of the general 2-D tracking loop are studied. Exact explicit expressions, taking into account the effects of local subcarrier waveform mismatching and the front-end bandlimiting, are provided for the correlation function employed in 2-D tracking. From these expressions, the key characteristics of 2-D correlation functions such as the shape, coupling relation between dimensions, and the effects of bandlimiting can be clearly seen. Moreover, general theoretical methods to predict the performance of the 2-D tracking techniques under the multipath and noise environments are provided. The results obtained in this paper can facilitate investigations in the area of 2-D tracking technique parameter optimization and performance assessment.

Manuscript received October 6, 2016; revised April 12, 2017 and July 5, 2017; released for publication July 5, 2017. Date of publication July 13, 2017; date of current version December 5, 2017.

DOI. No. 10.1109/TAES.2017.2726878

Refereeing of this contribution was handled by J. T. Curran.

This work was supported by the National Natural Science Foundation of China under Grant 61771272.

Authors addresses: Z. Yao, Y. Gao, and M. Lu are with the Department of Electronic Engineering, Tsinghua University, Beijing 100084, China, E-mail: (yaozheng@tsinghua.edu.cn; yangboy0811@163.com; lumq@tsinghua.edu.cn); Y. Gao is with Beijing Satellite Navigation Center, Beijing 100094, China, E-mail: (gaoy03@mails.tsinghua.edu.cn). (Zheng Yao and Yang Gao contributed equally to this work.) (Corresponding author: Zheng Yao.)

0018-9251 © 2017 IEEE

I. INTRODUCTION

Binary offset carrier (BOC) signals [1] will be widely used in new generation global navigation satellite systems (GNSS). A BOC signal can be regarded as a product of a direct sequence spread spectrum (DSSS) signal with rectangular chips and a square wave subcarrier. The modulation effect of the subcarrier moves the main spectrum component of BOC signals away from the carrier frequency, resulting in a spectrum separation from legacy signals located at the same central frequency and a wide root mean square bandwidth which means advantages on potential ranging accuracy and inherent multipath resisting ability. However, the price to pay for these potential performance improvements is a decrease in tracking reliability. Since a BOC signal has a sawtooth-like, piecewise linear auto-correlation function (ACF) having multiple peaks, during code tracking the loop may lock on one of the side peaks, resulting in an intolerable bias in pseudorange measurements. This is known as the *ambiguity threat* in BOC signals tracking, which is one of the challenging issues in the modernized multi-GNSS receiver [2]. In order to make the best use of the potential advantages of BOC signals for ranging and anti-multipath while avoiding the ambiguity problem, various unambiguous tracking methods have been proposed in recent years.

The existing unambiguous tracking methods of BOC signal can be divided into two classes for the treatment of the spreading code and the subcarrier. The first class of methods employs identical delay in the local code and subcarrier, and only one loop is used to track the variation of this delay [3]–[6]. This class of methods can be collectively referred to as the one-dimensional (1-D) tracking technique since the correlation function used is a 1-D function of delay. Besides 1-D tracking, there is another emerging class of unambiguous tracking methods in which the subcarrier and spreading code component are processed separately. More specifically, local replicas of the subcarrier and code use different delays and two independent loops are employed to track the variations of these two parameters. Representative existing methods in this class mainly include double estimate tracking (DET) [7]–[11], double phase estimator (DPE) [12], [13], and the robust unambiguous tracking method proposed in [14]. Since the correlation function used in these methods is a function of two variables, code delay and subcarrier delay, these methods can be collectively called the two-dimensional (2-D) tracking techniques. In recent years, new 2-D tracking techniques are emerging, such as decimation DPE [15] and Astrium correlator [16].

In the research of 2-D unambiguous tracking techniques, the general theories of tracking performance, especially when the dominant error sources are noise and multipath, are of great importance. On one hand, these theories can be used as the objective function to guide the optimization of key parameters. On the other hand, they can be used for performance comparison across different 2-D unambiguous tracking techniques. However, unlike the

1-D tracking case whose theoretical performance prediction methodologies have been developed quite well [17], 2-D tracking is still an emerging architecture, and its basic theories in performance prediction are currently not mature, mainly reflected in two aspects.

First, both the performance analysis and the selection of design parameters such as the local subcarrier, correlator spacing, and front-end bandwidth must be based on the knowledge of the cross-correlation function (CCF) between the received signal and the local replica. The semianalytic tracking loop simulations [18] are also based on this CCF. Nevertheless, in 2-D tracking, the correlation function is more complicated than that in 1-D cases, especially when the received signal is bandlimited. The key characteristics of the 2-D correlation function, such as the shape, coupling relation between dimensions, and the effects of bandlimiting, have not been understood thoroughly as of now. In previous work on basic 2-D tracking technique design, such as [8] and [9], the 2-D correlation function is oversimplified and only the infinite bandwidth case is considered. This leads to the result that some important characteristics of 2-D tracking cannot be reflected in theoretical performance prediction.

Second, the theoretical performance predicting methods for 2-D tracking have not been well established. The existing performance analysis is typically based on Monte-Carlo simulations [9] or on prototyping rather than on theoretical modeling. Relying solely on simulation cannot obtain universal results, and steady-state error variance statistics requires very long simulation cycles. In addition, in optimal parameter studies, the simulation has to be rerun each time a design parameter or input parameter is modified which is time consuming and computationally demanding. In [13], the approximate analytical results are obtained by applying the analysis methodology of 1-D tracking. However, due to the coupling property of 2-D CCF, the code loop and the subcarrier loop interact with each other. Ignoring the coupling relation between code tracking and subcarrier tracking may yield misleading results.

Corresponding to the above issues, the first main contribution of this paper is quantifying the key properties of the 2-D correlation function. The exact expressions of 2-D CCF and ACF of BOC signals, considering the effects of subcarrier waveform mismatching and front-end filtering, are proposed in this paper. Employing these expressions, 2-D correlation functions are understandable not only on the shape, but also on the coupling relation between dimensions, and the effects of bandlimiting. These results provide the basis for the theoretical analysis of 2-D loops.

Another main contribution of this paper is presenting the theoretical performance predicting methods of 2-D loops. Based on the results of 2-D CCF, the general theoretical prediction approaches of tracking jitter and multipath mitigation performance in 2-D tracking architecture are presented, in which both the cross-coupling effect and the bandlimiting effect are taken into account. The results allow a straightforward and unified theoretical analysis of the influence of different key design parameters such as the local subcarrier

waveform, bandwidth, code and subcarrier discriminators form, and early-late spacing on performance.

Furthermore, as application instances of the general theory, the noise and multipath theoretical performances of some representative 2-D unambiguous tracking techniques are analyzed by using the proposed methods. Some interesting results are shown for the first time, which not only reflect the distinctive feature of 2-D tracking compared to 1-D tracking, but also demonstrate the benefits of the proposed theoretical analysis approaches.

The organization of this paper is as follows. Section II formalizes the BOC signal model and the general 2-D tracking architecture. Section III presents the exact expressions of the 2-D correlation function of BOC signals under an arbitrary front-end bandwidth, and reveals the quantitative coupling relationship between the code delay and subcarrier delay dimensions. On the basis of results obtained in Section III, Sections IV and V propose the general theoretical predicting approaches of tracking jitter and multipath mitigation performance of 2-D tracking, respectively. In Section VI, with specific examples, the influence of different key parameters to the performance are shown and discussed. Finally, conclusions as well as the future work are discussed in Section VII. Appendices outline essential steps in deriving the expressions in this paper.

II. SIGNAL AND SYSTEM MODELS

A. BOC Signal Model

A GNSS radio-frequency (RF) signal at the antenna of the receiver can be modeled as

$$r(t) = \sqrt{2P}d(t - \tau)g(t - \tau)\cos(2\pi f_{RF}t + \varphi) + n(t) \quad (1)$$

where P is the signal power, $d(t)$ is the navigation message, $g(t)$ is the baseband DSSS component, τ is the signal propagation delay, f_{RF} and φ are the RF with the Doppler and the phase of the carrier respectively, and $n(t)$ is zero-mean Gaussian white noise introduced by the propagation channel, with power spectrum density N_0 . For BOC signals, $g(t)$ can be further formed as the product of two components, i.e.,

$$g_B(t) = g_c(t) \cdot b_B(t) \quad (2)$$

in which $g_c(t)$ is the spreading code component, and for a sine-phased BOC signal, $b_B(t) = \text{sgn}[\sin(2\pi f_{sc}t)]$ is a square wave subcarrier with frequency f_{sc} , where $\text{sgn}(x)$ is the sign function, which takes the value of 1 for $x \geq 0$ and -1 for $x < 0$.¹ The spreading code component $g_c(t)$ can be formed further as a series of time shifted and scaled

¹Note that BOC modulated signals can also take the cosine phase, the subcarrier of which is $\text{sgn}[\cos(2\pi f_{sc}t)]$. This paper mainly discusses the sine-phased BOC case. However, the derivation process and some of the results can be expanded to the cosine-phased BOC case straightforwardly.

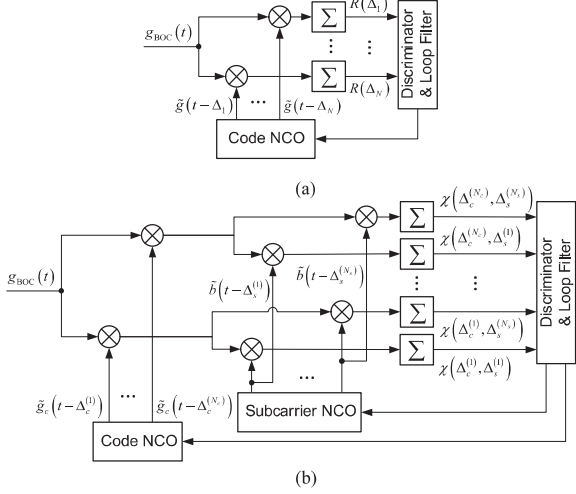


Fig. 1. Principal structures of (a) 1-D tracking loop and (b) 2-D tracking loop.

rectangular pulses

$$g_c(t) = \sum_{i=-\infty}^{\infty} c_i \Pi_{T_c}(t - iT_c) \quad (3)$$

where $\{c_i = \pm 1\}$ is the bipolar spreading sequence, and $\Pi_x(t)$ is a rectangular pulse which takes one for $0 \leq t < x$, and takes zero elsewhere.

Using the terminology from [1], a sine-phased BOC signal is denoted as $BOC_{sin}(m, n)$, where m is the ratio of f_{sc} to 1.023 MHz, and n represents the ratio of spreading code rate $f_c = 1/T_c$ to 1.023 MHz. m and n are constrained to positive integers, $m \geq n$, and the ratio $M = 2m/n$ is also a positive integer.

B. Canonical Model of 2-D Tracking Loop Processing

One of the main tasks of the receiver channel is to estimate τ from signal (1), which is usually done by code tracking loops.² This paper focuses on code tracking loops that satisfy the canonical forms illustrated in Fig. 1.

As shown in Fig. 1(a), in a 1-D tracking loop, components $g_c(t)$ and $b_B(t)$ are processed as a whole, and the essence of the loop is calculating the CCF between $g_B(t - \tau)$ and its local replica $\tilde{g}(t - \hat{\tau})$

$$R(\tau - \hat{\tau}) = \frac{1}{T} \int_0^T g_B(t - \tau) \tilde{g}(t - \hat{\tau}) dt \quad (4)$$

and maximizing it by adjusting the delay $\hat{\tau}$ of the local replica in a feedback loop. In (4), T is the integral length, and $T \gg T_c$. When the CCF reaches a maximum, it is considered that $\hat{\tau} \approx \tau$.

Different from 1-D tracking techniques, 2-D tracking techniques estimate the code delay τ_c and the subcarrier delay τ_s independently by using two separate loops. The final estimation of the signal delay $\hat{\tau}$ is obtained by a combination of the estimates of τ_c and τ_s . More specifically, in 2-D

²For the remainder of this paper, carrier loop is omitted and it is assumed that the carrier of the signal is removed ideally.

tracking techniques, as shown in Fig. 1(b), receivers generate local code components $\tilde{g}_c(t - \tau_c - \Delta_c^{(k)})$ with several different extra delays $\Delta_c^{(k)}$ for $k = 1, 2, \dots, N_c$, and local subcarrier components $\tilde{b}(t - \tau_s - \Delta_s^{(i)})$ with several different extra delays $\Delta_s^{(i)}$ for $i = 1, 2, \dots, N_s$, respectively. The products of $\tilde{g}_c(t - \tau_c - \Delta_c^{(k)})$ and $\tilde{b}(t - \tau_s - \Delta_s^{(i)})$ are correlated with the received signal to form a 2-D CCF

$$\chi(\tau - \tau_c - \Delta_c^{(k)}, \tau - \tau_s - \Delta_s^{(i)}) = \frac{1}{T} \int_0^T g_B(t - \tau) \tilde{g}_c(t - \tau_c - \Delta_c^{(k)}) \tilde{b}(t - \tau_s - \Delta_s^{(i)}) dt \quad (5)$$

which involves the bivariate function. With appropriate choices of $\Delta_c^{(k)}$ and $\Delta_s^{(i)}$, and combining correlation values observed at multiple points in the plane of the 2-D correlation surface, one can form discriminators which generate error signals, controlling two independent feedback loops to track τ_c and τ_s continuously.

Existing 2-D tracking techniques differ mainly in the selection of local replicas which affect the shape of the CCF, and the combination way of CCF samples in discriminators. The core of designing new 2-D tracking technique also lies in the choice of local waveforms and discriminator forms. Note that in order to despread successfully, the local code is always as same as that of the received signal, i.e., $\tilde{g}_c(t) = g_c(t)$. However, for a local subcarrier $\tilde{b}(t)$, the only constraint is that it should be a periodic signal with the same period as $b_B(t)$. The waveform of $\tilde{b}(t)$ can be the same as that of the received signal, as in [7], [10], and [16], or it can be a different waveform. For example, in [12] and [13], single sine wave subcarrier is employed instead of $b_B(t)$.

Specific discriminator forms in 2-D tracking techniques can also be varied [9], but essentially the outputs of all of these techniques are the estimation of tracking errors $\Delta\tau_c = \tau_c - \tau$ and $\Delta\tau_s = \tau_s - \tau$. A general form of the relationship functions between code discriminator output e_c , subcarrier discriminator output e_s , and tracking errors $\Delta\tau_c$ and $\Delta\tau_s$ can be expressed as

$$\begin{cases} e_c = \delta_c(\Delta\tau_c, \Delta\tau_s) + \epsilon_c \\ e_s = \delta_s(\Delta\tau_c, \Delta\tau_s) + \epsilon_s \end{cases} \quad (6)$$

where ϵ_c and ϵ_s are noises of code and subcarrier discrimination, respectively.

For all of the existing 2-D tracking techniques, the 2-D CCF (5) has a unique peak within a period of the spreading sequence in the code dimension, while it also has an infinite number of peaks with a period of $2T_s$ in the subcarrier dimension, where $T_s = 1/(2f_{sc})$. When both of these two loops are locked, the code loop can provide an unambiguous but noisier delay estimation $\hat{\tau}_c \approx \tau$, and the subcarrier loop can provide a high accuracy but ambiguous delay estimation $\hat{\tau}_s \approx \tau + NT_s$, where N is an arbitrary integer. An unambiguous and high-accuracy delay estimation can be obtained through the following formula:

$$\hat{\tau} = \hat{\tau}_s - \hat{N}T_s \quad (7)$$

where \hat{N} is the estimate of N , which can be obtained by several methods [7], [14].

III. ANALYTICAL 2-D CCF OF BOC SIGNALS

Based on the canonical form of the 2-D tracking loop, one can obtain various 2-D tracking techniques with different ranging accuracy, anti-multipath capability, and complexity through the selection of different $\tilde{b}(t)$, $\Delta_c^{(k)}$, $\Delta_s^{(i)}$, δ_c , and δ_s . The selection of these key parameters and front-end bandwidth must be based on the knowledge of the CCF shape. However, to the authors' knowledge, there is no available exact explicit expression of the 2-D CCF for BOC signals. Existing methods are based on numerical simulation, or are overly simplified, causing some of the important features to not be reflected in the performance prediction of 2-D tracking. In this section, exact explicit expressions of that 2-D CCF with both the infinite and limited bandwidths are given. For each case, generalized local subcarrier waveforms are considered, after which, as a special case, the 2-D ACF expressions of BOC signals, are also given. For the bandlimited case, we further provide the 2-D CCF with a sine wave local subcarrier. The results of this part are the basis of the performance study and design parameter selection of 2-D tracking techniques. For concision and without loss of generality, hereafter, if there is no special note, we always assume that $\tau = 0$, which yields $\Delta\tau_c = \tau_c$ and $\Delta\tau_s = \tau_s$.

A. Infinite Bandwidth

1) *General Form:* We first consider a most general case, where the local subcarrier $\tilde{b}(t)$ is an arbitrary periodic signal with period $2T_s$, which can be represented as $\tilde{b}(t) = \sum_{n=-\infty}^{\infty} \tilde{q}(t - 2nT_s)$, and $\tilde{q}(t)$ is nonzero only when $t \in [0, 2T_s]$. Then, the 2-D CCF with infinite bandwidth can be written as

$$\chi(\tau_c, \tau_s) = \frac{1}{T} \int_0^T g_c(t) b_B(t) g_c(t - \tau_c) \tilde{b}(t - \tau_s) dt. \quad (8)$$

With the assumption that the autocorrelation characteristic of $\{c_i\}$ is approximately ideal which is reasonable when the sequence period is large enough, as shown in Appendix A, (8) can be simplified as the 2-D CCF of chip pulses and subcarrier waveforms

$$\chi(\tau_c, \tau_s) = \frac{1}{T_c} \int_0^{T_c} \Pi_{T_c}(t - \tau_c) b_B(t) \tilde{b}(t - \tau_s) dt. \quad (9)$$

The integral in (9) is nonzero only when $|\tau_c| < T_c$, and it is easy to show that $\chi(\tau_c, \tau_s) = \chi(\tau_c, \tau_s + 2nT_s)$. Therefore, only the ranges $|\tau_s| < T_s$ and $|\tau_c| < T_c$ need to be taken into account in the following discussion.

2) *Odd Harmonic Local Subcarrier Case:* If $\tilde{b}(t)$ is an odd harmonic function, i.e., $\tilde{q}(t) = \tilde{q}_0(t) - \tilde{q}_0(t - T_s)$, in which $\tilde{q}_0(t)$ is nonzero only when $t \in [0, T_s]$, then as shown in Appendix A, (9) can be further simplified into

$$\chi(\tau_c, \tau_s) = \frac{1}{T_c} \left[aR_1(\tau_s) + R_2\left(\tau_s + \frac{T_s}{2}(1 - \text{sgn}(\tau_c)); \varepsilon\right) \right] \quad (10)$$

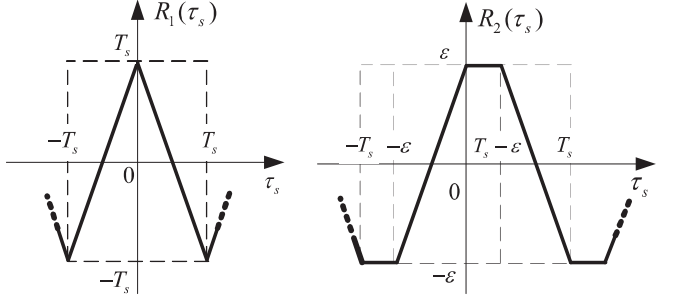


Fig. 2. function waveforms of $R_{1,B}(\tau_s)$ and $R_{2,B}(\tau_s)$.

where $a = \lfloor (T_c - |\tau_c|) / T_s \rfloor$, $\varepsilon = T_c - |\tau_c| - kT_s$, and

$$\begin{cases} \Gamma(t; \tau_s) = \tilde{q}_0(t - \tau_s) - \tilde{q}_0(t - \tau_s + T_s \text{sgn}(\tau_s)) \\ R_1(\tau_s) \triangleq \int_0^{T_s} \Gamma(t; \tau_s) dt \\ R_2(\tau_s; \varepsilon) \triangleq \int_0^{\varepsilon} \Gamma(t; \tau_s - T_s) dt. \end{cases} \quad (11)$$

If $\tilde{q}_0(t)$ is further symmetrical with respect to $T_s/2$, i.e., $\tilde{q}_0(t) = \tilde{q}_0(T_s - t)$, the 2-D CCF can be expressed in a more concise form

$$\chi(\tau_c, \tau_s) = \frac{1}{T_c} [aR_1(\tau_s) + R_2(\tau_s \text{sgn}(\tau_c); \varepsilon)]. \quad (12)$$

Almost all of local subcarrier waveforms employed by existing 2-D tracking techniques can satisfy the last case, for which the 2-D CCF under the infinite bandwidth can be completely described by the first quarter of the subcarrier $\tilde{q}_0(t)$ via (12).

3) *2-D ACF of BOC_{sin}(βn, n) Signals With Infinite Bandwidth:* As a special case of 2-D CCF, when $\tilde{b}(t) = b_B(t)$, i.e., $\tilde{q}_0(t) = \Pi_{T_s}(t)$, using (12), the analytic 2-D ACF expression of BOC_{sin}(βn, n) signals with infinite bandwidth in the interval $|\tau_s| \leqslant T_s$ and $|\tau_c| < T_c$ can be obtained:

$$\chi_B(\tau_c, \tau_s) = \frac{1}{T_c} [aR_{1,B}(\tau_s) + R_{2,B}(\tau_s \text{sgn}(\tau_c); \varepsilon)] \quad (13)$$

where, as illustrated in Fig. 2, both of $R_{1,B}(\tau_s)$ and $R_{2,B}(\tau_s)$ are piecewise linear functions, the expressions of which within $|\tau_s| \leqslant T_s$ are $R_{1,B}(\tau_s) = T_s - 2|\tau_s|$ and

$$R_{2,B}(\tau_s; \varepsilon) = \begin{cases} -\varepsilon, & -T_s \leqslant \tau_s < -\varepsilon \\ \varepsilon + 2\tau_s, & -\varepsilon \leqslant \tau_s < 0 \\ \varepsilon, & 0 \leqslant \tau_s < T_s - \varepsilon \\ 2T_s - \varepsilon - 2\tau_s, & T_s - \varepsilon \leqslant \tau_s \leqslant T_s \end{cases} \quad (14)$$

respectively. Numerical tests show that the maximum error between (13) and the real 2-D autocorrelation calculated by using GPS C/A code is less than 0.1%. The error is due to the nonideal correlation features of the spreading sequence.

The analytic expression (13) can be expanded to the whole $\tau_s \in \mathbb{R}$ by periodic extension. Fig. 3 (a)-(c) shows the 2-D ACF of a BOC_{sin}(4, 1) signal with unlimited bandwidth in three different aspects.

From the results obtained, one can see some important phenomena which have not been noted before. Although

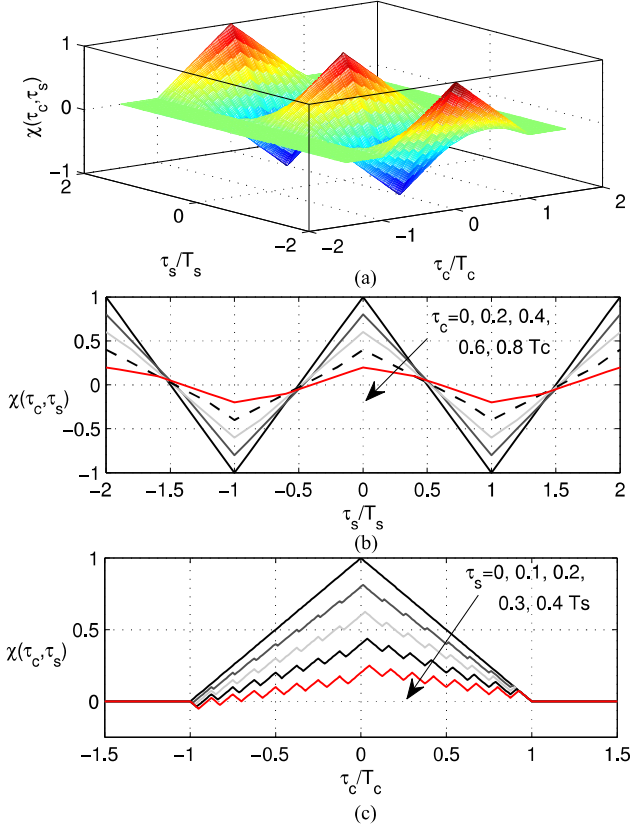


Fig. 3. Two-dimensional ACF of $\text{BOC}_{\sin}(4, 1)$ signal with unlimited bandwidth, (a) oblique drawing, (b) profile in τ_s dimension with $\tau_c = 0, 0.2T_c, 0.4T_c, 0.6T_c$, and $0.8T_c$, (c) profile in τ_c dimension with $\tau_s = 0, 0.1T_s, 0.2T_s, 0.3T_s$, and $0.4T_s$.

the 2-D ACF roughly presents a triangular peak in code delay dimension and presents a triangular wave in subcarrier delay dimension, from the exact expression (13) and the profiles shown in Fig. 3, we can clearly see that in $\chi_B(\tau_c, \tau_s)$, there is a complex coupling between the code delay and subcarrier delay dimensions. When $\tau_c = 0$, in τ_s dimension $\chi_B(0, \tau_s)$ is a periodic triangular wave and is symmetric about $\tau_s = kT_s, \forall k \in \mathbb{Z}$. However, as τ_c takes on a nonzero value, this periodic triangular wave is distorted and its symmetry is broken. A similar phenomenon is also in the τ_c dimension: When $\tau_s = 0$, $\chi_B(\tau_c, 0)$ has a symmetric triangular peak. Nevertheless, as τ_s takes on a nonzero value, this peak becomes distorted and asymmetric. Thanks to the exact analytic expression (13), the degree of these distortions can be quantified accurately.

B. Band Limited

1) *General Form:* Considering the bandwidth constraint, the 2-D CCF (9) should be rewritten as

$$\tilde{\chi}(\tau_c, \tau_s) = \frac{1}{T_c} \int_0^{T_c} [b_B(t) * h(t)] \Pi_{T_c}(t - \tau_c) \tilde{b}(t - \tau_s) dt \quad (15)$$

where $h(t)$ is the unit impulse response of the low-pass filter with one-sided bandwidth β_r , whose frequency response function $H(f)$ takes a value of one for $|f| < \beta_r$ and a value of zero elsewhere. By introducing the Fourier

transform (FT) of truncated time-shift subcarrier waveforms $B_B^{(t_0)}(f) \triangleq \mathcal{F}\{b_B(t - t_0) \Pi_{T_c}(t)\}$ and $\tilde{B}^{(t_0)}(f) \triangleq \mathcal{F}\{\tilde{b}(t - t_0) \Pi_{T_c}(t)\}$, (15) becomes

$$\tilde{\chi}(\tau_c, \tau_s) = \frac{1}{T_c} \int_{-\beta_r}^{\beta_r} B_B^{(0)}(f) \tilde{B}^{(\tau_s - \tau_c)*}(f) e^{j2\pi f \tau_c} df. \quad (16)$$

Since the truncated FT of BOC subcarrier waveform $b_B(t)$ is

$$B_B^{(0)}(f) = T_c \frac{\operatorname{sinc}(\pi f T_c) \tan(\pi f T_s)}{e^{j2\pi(f T_c - \frac{1}{4})}}, |t_0| \leqslant T_s \quad (17)$$

where $\operatorname{sinc}(x) \triangleq \sin(x)/x$, the 2-D CCF under the bandwidth constraint relies on the local subcarrier waveform $\tilde{b}(t)$ and the bandwidth β_r via (16). Alterations to $\tilde{b}(t)$ or β_r will change the shape of the 2-D CCF, thereby changing the noise and multipath performances of the loop.

Two cases of $\tilde{b}(t)$ we are most interested in $\tilde{b}(t) = b_B(t)$ and $\tilde{b}(t) = \sin(2\pi f_{sc} t)$, which correspond to local subcarriers employed in [7], [10], [16] and [12], [13], respectively.

2) *2-D ACF of Band-Limiting $\text{BOC}_{\sin}(\beta n, n)$ Signals:* When $\tilde{b}(t) = b_B(t)$, substituting $\tilde{B}^{(t_0)}(f) = B_B^{(t_0)}(f)$ into (16), after some algebraic manipulation, we can obtain the exact expression of 2-D ACF of bandlimiting $\text{BOC}_{\sin}(\beta n, n)$ signals,

$$\begin{aligned} \tilde{\chi}_B(\tau_c, \tau_s) = & \int_{-\beta_r}^{\beta_r} \frac{\eta(f)}{\tan(\pi f T_s)} \{ \cos(2\pi f [\Lambda(\tau_c - \tau_s) - \tau_c]) \\ & - [\sin(2\pi f [\Lambda(\tau_c - \tau_s) - \tau_c]) + \sin(2\pi f \tau_c)] \\ & \times \operatorname{sgn}(\Lambda(\tau_c - \tau_s)) \} df \end{aligned} \quad (18)$$

where $\eta(f) \triangleq T_c \tan^2(\pi f T_s) \operatorname{sinc}^2(\pi f T_c)$ is the power spectral density of BOC signal, and $\Lambda(t) \triangleq t - \lfloor f_{sc}t + \frac{1}{2} \rfloor$ is the sawtooth wave with periodic $2T_s$.

Taking the $\text{BOC}_{\sin}(4, 1)$ signal as an example, Fig. 4(a)–(c) shows the bandlimiting 2-D ACF in three different aspects, where $\beta_r = 5.115$ MHz.

It can be seen from Fig. 4 that, similar to the infinite bandwidth case, in bandlimiting 2-D ACF, there is also complex coupling between the two dimensions. When $\tau_c = 0$, in τ_s dimension $\tilde{\chi}_B(0, \tau_s)$ is symmetric about $\tau_s = kT_s, \forall k \in \mathbb{Z}$. However, as τ_c takes nonzero value, its symmetry is broken. A similar phenomenon is also in the τ_c dimension: when $\tau_s = 0$, $\tilde{\chi}_B(\tau_c, 0)$ has a symmetric peak. Nevertheless, as τ_s takes a nonzero value, this peak becomes distorted and asymmetric.

3) *2-D CCF With Sine Wave Local Subcarrier:* When $\tilde{b}(t) = \sin(2\pi f_{sc} t)$, the exact expression of 2-D CCF of the $\text{BOC}_{\sin}(\beta n, n)$ signal and its replica with sine wave subcarrier is

$$\begin{aligned} \tilde{\chi}_{\sin}(\tau_c, \tau_s) = & \int_{-\beta_r}^{\beta_r} \frac{f \eta(f)}{2 \tan(\pi f T_s)} \left[\frac{\cos[2\pi(f_{sc}(\tau_c - \tau_s) + f \tau_c)]}{f + f_{sc}} \right. \\ & \left. - \frac{\cos[2\pi(f_{sc}(\tau_c - \tau_s) - f \tau_c)]}{f - f_{sc}} \right] df. \end{aligned} \quad (19)$$

It has the similar coupling phenomenon as in the 2-D ACF. The profiles of this case are not provided here due to the space limitation.

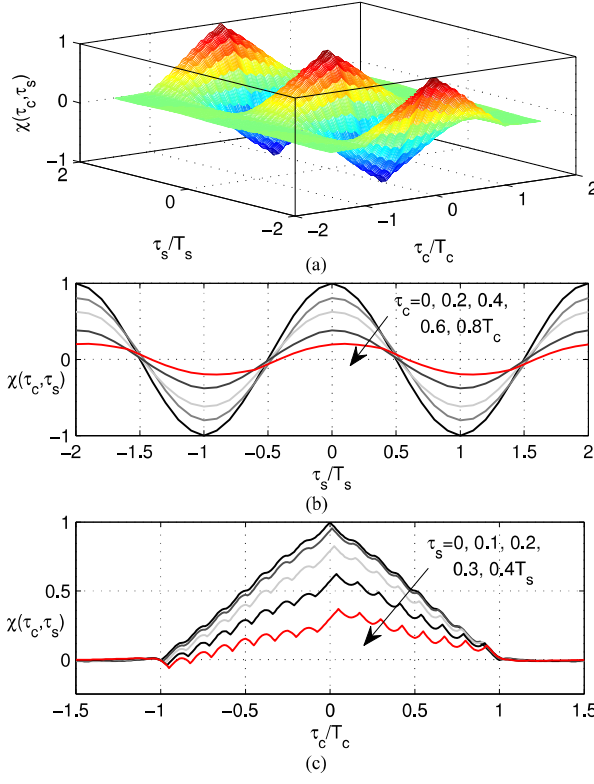


Fig. 4. Bandlimiting 2-D ACF of $\text{BOC}_{\text{sin}}(4, 1)$ signal, where $\beta_r = 5.115 \text{ MHz}$, (a) oblique drawing, (b) profile in τ_s dimension with $\tau_c = 0, 0.2T_c, 0.4T_c, 0.6T_c$, and $0.8T_c$, (c) profile in τ_c dimension with $\tau_s = 0, 0.1T_s, 0.2T_s, 0.3T_s$, and $0.4T_s$.

C. Summary

The benefits of accurate expressions to the 2-D CCF of BOC signals with both limited and unlimited bandwidth are multifold. First, as explicit expressions, they are convenient. Explicit CCF allows the algorithm to be designed in an analytical way. More general and parameterized results can be obtained. Second, tracking performance analysis based on these simple functions needs significantly less computational complexity compared to numerical simulation, especially in the comparative studies of varying input parameters. Finally, the explicit CCF also produces valuable geometrical insight into the problem.

As shown above, thanks to the exact expressions (13), (18), and (19), the coupling between the two dimensions can be quantified accurately. Because of this nonnegligible complex coupling relationship, whether in noise performance analysis, in multipath performance analysis, or in loop optimal parameters selection, the code tracking loop and the subcarrier tracking loop cannot be discussed independently, therefore the 1-D tracking results should not be directly applied to 2-D tracking. Therefore, it is necessary to provide dedicated methods for 2-D loop performance analysis.

In the following two sections, the expressions of 2-D CCF are used to support the general analysis of 2-D loops performance in terms of tracking jitter and multipath mitigation. From the processes of analysis, the benefits of analytic expressions presented above can be further embodied.

IV. GENERAL NOISE PERFORMANCE ANALYSIS METHOD FOR 2-D LOOPS

When thermal noise is present, the relationship between the outputs of general discriminators and the actual errors τ_c and τ_s can be expressed by (6). Consistent with most analyses of tracking accuracy, it is assumed that the joint discriminator of τ_c and τ_s is unbiased, i.e., $\delta_c(0, 0) = \delta_s(0, 0) = 0$. Linearizing (6) around $\tau_c = \tau_s = 0$ yields

$$\begin{cases} e_c \approx \kappa_{cc}\tau_c + \kappa_{cs}\tau_s + \epsilon_c \\ e_s \approx \kappa_{sc}\tau_c + \kappa_{ss}\tau_s + \epsilon_s \end{cases} \quad (20)$$

where

$$\kappa_{ij} = \left. \frac{\partial \delta_i(\tau_c, \tau_s)}{\partial \tau_j} \right|_{\tau_c=\tau_s=0}, \text{ for } i, j \in \{c, s\} \quad (21)$$

are discriminator slopes which reflect the sensitivity of discriminators to errors. We denote

$$\mathbf{K} = \begin{bmatrix} \kappa_{cc} & \kappa_{cs} \\ \kappa_{sc} & \kappa_{ss} \end{bmatrix} \quad (22)$$

as the slope matrix. Then, the covariance matrix of the open-loop estimations of $[\tau_c, \tau_s]^T$ can be obtained by

$$\mathbf{Q} = \begin{bmatrix} q_c & q_{cs} \\ q_{sc} & q_s \end{bmatrix} = \mathbf{K}^{-1} \mathbf{N} (\mathbf{K}^{-1})^T \quad (23)$$

where \mathbf{N} is the covariance matrix of $[\epsilon_c, \epsilon_s]^T$ in which $n_{cc} = \text{var}\{\epsilon_c\}$, $n_{ss} = \text{var}\{\epsilon_s\}$, and $n_{cs} = E\{\epsilon_c \epsilon_s\}$. If the final delay estimation is calculated through (7), the open-loop delay estimation accuracy is only dependent on the estimation accuracy of τ_s , with variance q_s . By using the relationship between open-loop accuracy and closed-loop accuracy given in [17], we can obtain the closed-loop delay estimation variance

$$\begin{aligned} \sigma_\tau^2 &= 2q_s B_L T (1 - 0.5B_L T) \\ &= \frac{2(\kappa_{sc}^2 n_{cc} + \kappa_{cc}^2 n_{ss} - 2\kappa_{sc}\kappa_{cc}n_{cs}) B_L T (1 - 0.5B_L T)}{(\kappa_{cc}\kappa_{ss} - \kappa_{sc}\kappa_{cs})^2} \end{aligned} \quad (24)$$

where B_L is the one-sided equivalent loop bandwidth.

In the general noise performance analysis method of 2-D loops discussed above, the key to obtain closed-loop error variance (24) is calculating the slope matrix \mathbf{K} and the covariance matrix \mathbf{N} , where the former depends on the specific form of discriminators, and the latter depends on the corresponding noise characteristics. With different discriminators, the specific form of these two matrices can be different. However, both of them are closely related to the 2-D CCF and are influenced by its coupling between two dimensions.

Specifically, the coupling effect is reflected by the nondiagonal entries of slope matrix \mathbf{K} , i.e., κ_{sc} and κ_{cs} . It is interesting that if $\kappa_{sc} = \kappa_{cs} = 0$, which meant the coupling effect disappears, (24) would become $\sigma_\tau^2 = n_{ss} B_L T (1 - 0.5B_L T)$, which would correspond to the traditional noise performance analysis expression in 1-D loops. However, in Section VI, with some specific

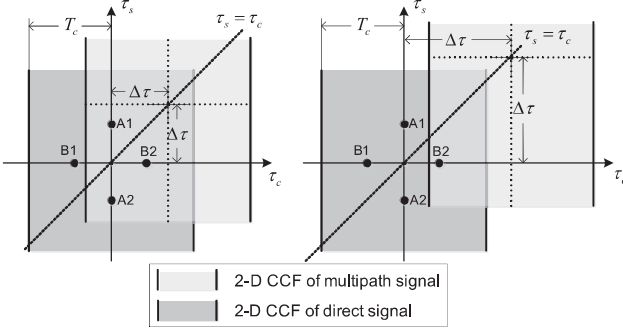


Fig. 5. Influence of multipath in 2-D tracking diagrams: Direct influence (left), and indirect influence (right).

examples, we will see that the existence of the coupling effect leads to different performance from 1-D tracking.

V. GENERAL MULTIPATH PERFORMANCE ANALYSIS METHOD FOR 2-D LOOPS

A common way of assessing antimultipath performance is based on the computation of the multipath error envelope [19]. This assessment represents the influence of one single multipath signal with a given relative amplitude α that is constant for all considered geometric path delays. Neglecting the effect of noise, a received signal with multipath after frequency down conversion can be expressed as $s(t) = g_{BOC}(t) + \alpha \cos \phi g_{BOC}(t - \Delta\tau)$, where ϕ and $\Delta\tau$ are the relative carrier phase and relative propagation delay of the multipath component, respectively. After correlation with the product of the local code and the local subcarrier employing separate delays, the 2-D CCF of the received signal contaminated by multipath is

$$\chi_{mp}(\tau_c, \tau_s) = \chi(\tau_c, \tau_s) + \alpha \cos \phi \chi(\tau_c - \Delta\tau, \tau_s - \Delta\tau). \quad (25)$$

This multipath contamination can be represented graphically. In Fig. 5, the 2-D CCF top views of the direct signal and that of the multipath are shown as dark gray and light gray banded areas, respectively. Two black border lines in code dimension indicate that $\chi(\tau_c, \tau_s)$ is nonzero only when $|\tau_c| < T_c$. However, since $\chi(\tau_c, \tau_s)$ is periodic in the subcarrier dimension, there is no border line in that dimension. A_1 and A_2 represent two correlation values employed in the subcarrier discriminator, when B_1 and B_2 are two correlation values used in the code discriminator. Specifically, if there is no multipath, they can be written as $A_1 = \chi(\tau_c, \tau_s + \frac{\Delta_s}{2})$, $A_2 = \chi(\tau_c, \tau_s - \frac{\Delta_s}{2})$, $B_1 = \chi(\tau_c + \frac{\Delta_c}{2}, \tau_s)$, and $B_2 = \chi(\tau_c - \frac{\Delta_c}{2}, \tau_s)$. Note that in this two-dimensional graphic, the multipath delay $\Delta\tau$ can only change along the diagonal $\tau_s = \tau_c$ in the positive direction. With the superposition of 2-D CCF for multipath, one or more correlation values will be contaminated, so that the code and subcarrier discriminators may be distorted.

Taking into account the influence of multipath, the relationship between discriminator outputs and tracking errors (6) can be rewritten as

$$\begin{cases} e_c^m = \delta_c^m(\tau_c, \tau_s) \\ e_s^m = \delta_s^m(\tau_c, \tau_s) \end{cases} \quad (26)$$

where the superscript m indicates the multipath contamination. The computation of the multipath-induced error is equivalent to finding the points where the discriminator curves cross the origin, with given α, ϕ , and $\Delta\tau$. That is

$$[\varepsilon_c, \varepsilon_s]^T = \arg \left\{ \begin{cases} \delta_c^m(\tau_c, \tau_s) = 0 \\ \delta_s^m(\tau_c, \tau_s) = 0 \end{cases} \right\}. \quad (27)$$

The iterative method can be used to solve these nonlinear equations. First, for a given α, ϕ , and $\Delta\tau$, with a current approximate solution $[\tau_c^i, \tau_s^i]^T$, these two equations can be linearized as

$$\begin{cases} \delta_c^m(\tau_c^i, \tau_s^i) + \kappa_{cc}^i \Delta\tau_c^i + \kappa_{cs}^i \Delta\tau_s^i = 0 \\ \delta_s^m(\tau_c^i, \tau_s^i) + \kappa_{sc}^i \Delta\tau_c^i + \kappa_{ss}^i \Delta\tau_s^i = 0 \end{cases} \quad (28)$$

where $\kappa_{jk}^i = \partial \delta_j^m(\tau_c, \tau_s) / \partial \tau_k \Big|_{\tau_c=\tau_c^i, \tau_s=\tau_s^i}$, for $j, k \in \{c, s\}$.

In (28), κ_{sc}^i and κ_{cs}^i reflect the mutual influence of multipath errors in code and subcarrier discriminators. Solving (28) gives $\Delta\tau_c^i$ and $\Delta\tau_s^i$. By letting $\tau_c^{i+1} = \tau_c^i + \Delta\tau_c^i$ and $\tau_s^{i+1} = \tau_s^i + \Delta\tau_s^i$, calculating new $\Delta\tau_c^{i+1}$ and $\Delta\tau_s^{i+1}$, and so on, the process can be repeated until it converges to a pair of fixed points $[\tau_c^n, \tau_s^n]^T$, which are the multipath errors of the code tracking and subcarrier tracking, respectively. The final multipath error of delay estimation is τ_s^n . Note that with the explicit expression of 2-D CCF, κ_{jk}^i can be presented as the explicit form with respect to τ_c^i and τ_s^i , thus the derivative calculation is not actually required in each iteration. Moreover, in general, the iteration number of the above analysis method does not need to be large. For most 2-D tracking techniques with relatively regular discriminator curves, such as DET and DPE, good convergence effects can be obtained in a single step iteration. Therefore, compared to numerical simulation, the proposed multipath performance analysis method needs significantly less computational complexity, especially when multiple parameters need to be traversed.

Compared to the antimultipath performance analysis of 1-D loop, a key difference in that of 2-D loop is the coupling effect between the two discriminators. In (28), both κ_{sc}^i and κ_{cs}^i are not zero. The interaction between the code and subcarrier discriminators makes the 2-D loop show more complex properties, as discussed based on some specific cases in the following section.

VI. CASE STUDIES

This section provides some case studies to examine the behavior of the expressions and performance analysis methods presented in the preceding section of this paper. There are two primary purposes of these case studies.

- 1) Demonstrating how to implement the proposed general theoretical performance predicting methods in specific 2-D tracking techniques and showing the role of the proposed methods in performance assessment and parameter selection.
- 2) Presenting some important results of 2-D tracking having not been reported in the previous literature, that can

not only reflect the distinctive feature of 2-D tracking compared to 1-D tracking, but also show the benefits of the proposed methods.

Two different effects are explored in each case study. The first set of results considers the coupling effect between the code tracking loop and subcarrier tracking loop, thus exploring the effect of code early-late spacing selection on subcarrier tracking performance. The second set of results examines the effect of bandlimiting and subcarrier early-late spacing on tracking performance.

Owing to space limitations, this section could not cover the results for all the existing 2-D tracking techniques. Two representative 2-D tracking techniques, DET and DPE, are considered. However, with the corresponding $\tilde{b}(t)$, δ_c , and δ_s , the analysis process of these case studies can be applied to the other 2-D tracking loops directly.

A. Case Study: Noise Performances of DET and DPE in Bandlimiting Case

In this section, the jitter performances of DET and DPE, for bandlimited $\text{BOC}_{\sin}(2, 1)$ signals, are discussed as specific examples.

Applying the 2-D loop canonical model, in DET, $\tilde{b}(t) = b_B(t)$, $N_c = N_s = 2$, $\Delta_c^{(1)} = \Delta_c/2$, $\Delta_c^{(2)} = -\Delta_c/2$, $\Delta_s^{(1)} = \Delta_s/2$, $\Delta_s^{(2)} = -\Delta_s/2$, and

$$\begin{cases} \delta_c = \tilde{\chi}_B(\tau_c - \Delta_c^{(1)}, \tau_s) - \tilde{\chi}_B(\tau_c - \Delta_c^{(2)}, \tau_s) \\ \delta_s = \tilde{\chi}_B(\tau_c, \tau_s - \Delta_s^{(1)}) - \tilde{\chi}_B(\tau_c, \tau_s - \Delta_s^{(2)}) \end{cases} \quad (29)$$

where Δ_c and Δ_s are the spacing between early and late replicas for the code discriminator and the subcarrier discriminator, respectively, and are assumed to be in the ranges $0 < \Delta_c \leq T_c$ and $0 < \Delta_s \leq T_s$. In DPE, $\tilde{b}(t) = \sin(2\pi f_{sc}t)$, $N_c = 2$, $N_s = 1$, $\Delta_c^{(1)} = \Delta_c/2$, $\Delta_c^{(2)} = -\Delta_c/2$, $\Delta_s^{(1)} = T_s/2$, and

$$\begin{cases} \delta'_c = \tilde{\chi}_{\sin}(\tau_c - \Delta_c^{(1)}, \tau_s) - \tilde{\chi}_{\sin}(\tau_c - \Delta_c^{(2)}, \tau_s) \\ \delta'_s = \tilde{\chi}_{\sin}(\tau_c, \tau_s - \Delta_s^{(1)}) \end{cases} \quad (30)$$

The derivation of δ_c , δ_s , and the entries of \mathbf{K} and \mathbf{N} are provided in Appendix B, in which two points require special attention. First, for both DET and DPE, τ_c exists in the right-hand side of $\delta_s(\tau_c, \tau_s)$, and τ_s exists in the right-hand side of $\delta_c(\tau_c, \tau_s)$, thus the nondiagonal entries elements of \mathbf{K} are nonzero, which implies that the code discriminator and the subcarrier discriminator interact with each other. Second, for the code discriminator in both DET and DPE, different early-late spacing results in different discriminator curve shapes. Especially when Δ_c is close to an even multiple of T_s , the code discriminator slope becomes very small.

1) *Influence of Coupling Effect:* Fig. 6 shows the closed-loop tracking error theoretical standard deviations of DET and DPE predicted by (24), where the one-sided front-end filter bandwidth employed is $\beta_r = 3f_c$, which is just large enough to contain two main lobes of the $\text{BOC}_{\sin}(2, 1)$ signal spectrum, the loop bandwidth is $B_L = 1$ Hz, and the subcarrier early-late spacing is $\Delta_s = 0.2T_s$. The code early-late spacings we chose are $\Delta_c = iT_s$, where $i = 2, 3, 4, 5$.

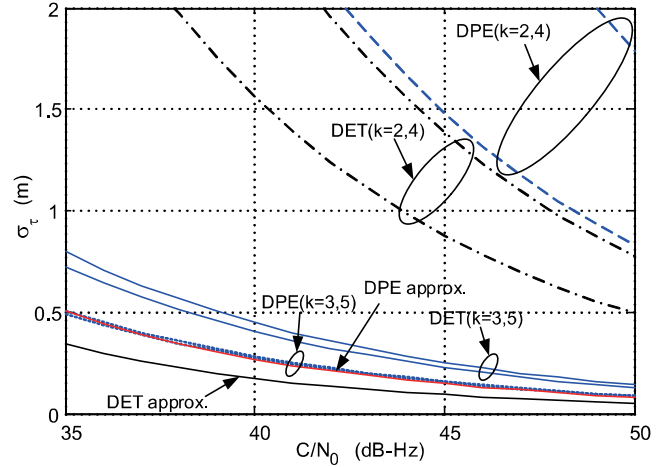


Fig. 6. Tracking jitters of DET and DPE with different code early-late spacing $\Delta_c = iT_s$, $i = 2, 3, 4, 5$.

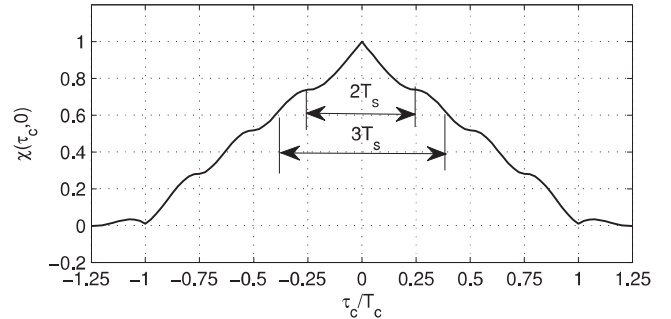


Fig. 7. Profile of the bandlimited $\text{BOC}_{\sin}(2, 1)$ signal ACF in τ_c dimension with $\tau_s = 0$.

For comparison, the 1-D approximate results, predicted by the expressions provided in [13] [(30) and (32)], are also shown in this figure, under the same parameter conditions. Note that in these approximate expressions, results are independent of Δ_c and β_r .

From the results predicted by the exact expression (24), it can be seen that the selection of Δ_c significantly affects the final ranging accuracy. For both of DET and DPE, the tracking accuracy with Δ_c confined to odd multiples of T_s (i.e., $k = 3, 5$) is generally better than that with Δ_c confined to even multiples of T_s (i.e., $k = 2, 4$). At first glance, these results are somewhat counterintuitive, since the final ranging accuracy is mainly determined by the subcarrier loop tracking accuracy. In most of the previous studies ignoring the coupling of two loops, the code early-late spacing parameter does not appear in the tracking error expression, so this phenomenon cannot be fully exposed. However, using the 2-D CCF exact expressions and the proposed theoretical analysis method, this phenomenon can be observed and its mechanism can be clearly explained.

The profile of the bandlimited $\text{BOC}_{\sin}(2, 1)$ signal ACF in τ_c dimension with $\tau_s = 0$ is plotted in Fig. 7 via (18). We can notice that at those τ_c closest to an odd multiple of T_s , the absolute value of the correlation function slope reaches its maximum, which means a higher code

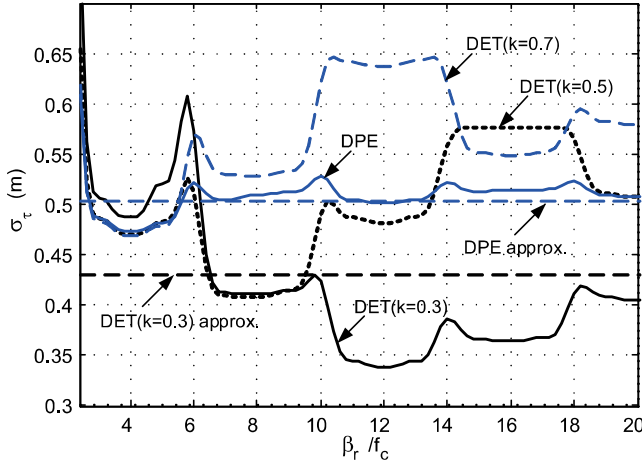


Fig. 8. Tracking jitters of DET and DPE with different subcarrier early-late spacing $\Delta_s = kT_s$, ($k = 0.3, 0.5, 0.7$) at carrier-to-noise ratio of 35 dB-Hz and $\Delta_c = T_s$.

discriminator gain. In the opposite case, where τ_c is closest to an even multiple of T_s , the absolute value of the correlation function slope is extremely low, resulting in a low code discriminator gain. This observation is consistent with the result proved strictly in Appendix B, that for both DET and DPE, $\kappa_{cc} \approx 0$ when Δ_c is close to an even multiple of T_s . Therefore, when an even multiple of T_s is chosen as the code early-late spacing, the code discriminator will be insensitive to the delay variation, resulting in a greater code tracking jitter. Although the final delay estimation accuracy is determined by the subcarrier loop tracking accuracy, due to the coupling between code tracking and subcarrier tracking in the 2-D loop structure, the performance degradation of code tracking loop ultimately affects the delay estimation accuracy. The same is true with DPE, the 2-D CCF employed by which is described by (19).

Therefore, in order to achieve better tracking performance, the code early-late spacing Δ_c should be set near to an odd multiple of T_s rather than an even multiple of T_s . Although the discussion above is based on the condition of $\text{BOC}_{\sin}(2, 1)$, by using (24) under the other parameter conditions, it is easy to verify that the conclusion we draw is applicable for all of the bandlimited BOC signals.

From Fig. 6 we can also find that the 1-D approximate expression for DPE provided in [13] agrees with the exact expression well for odd k cases, though it cannot reflect the performance of DPE for even k cases. However, with the given β_r and Δ_s in this set of results, the 1-D approximate expression for DET has a relatively large deviation from the exact expression, which is mainly because of the sensitivity of the DET tracking accuracy to the bandwidth.

2) *Influence of Bandlimiting:* Fig. 8 shows the tracking error of DET and DPE with various values of subcarrier early-late spacing, with respect to the normalized front-end filter bandwidth β_r/f_c . In this figure, Δ_c is fixed at T_s , and the carrier-to-noise ratio is fixed at 35 dB-Hz. The subcarrier early-late spacing of DET we chose are $\Delta_s = kT_s$, where $k = 0.3, 0.5, 0.9$. The other parameter conditions are the same as for the

previous part. For comparison, the 1-D approximate result of DPE and DET for $k = 0.3$, predicted by [13] (30) and (32), respectively, are also shown in this figure as two horizontal lines, independent of β_r .

From Fig. 8, we can see that the tracking performance of DPE fluctuates little with the bandwidth, and the approximate expression is in good agreement with the exact expression for most bandwidth conditions. However, the tracking error of DET is obviously influenced by β_r and Δ_s . Under a certain Δ_s , the tracking error of DET fluctuates with β_r significantly, so that the 1-D approximate expression for DET, which ignores the effect of the front-end bandwidth, cannot reflect the performance exactly.

It can also be observed that when the front-end bandwidth is just wide enough for two main lobes and at most one pair of sidelobes of the BOC signal spectrum to get through, there is no significant tracking performance difference for loops with $\Delta_s > 0.5T_s$. A smaller Δ_s may even result in a worse tracking performance. In such a bandwidth-limited situation, DPE has better tracking accuracy than DET. However, as bandwidth increases, the DET performance difference due to Δ_s becomes more significant. As shown in Fig. 8, for a $\text{BOC}_{\sin}(2, 1)$ signal, when the bandwidth is between 7 and 9 MHz, DET with $\Delta_s = 0.3T_s$ and $0.5T_s$ can obtain a better tracking accuracy than DPE. With wider β_r , the tracking accuracy of DET with $\Delta_s = 0.3T_s$ can be further improved.

Since the optimal discriminator form and correlation spacing are bandwidth-dependent, the above analysis method and results can provide guidance to receiver designers in the selection of these key design parameters.

B. Case Study: Multipath Performance of DET in BandLimiting Case

As a specific example, in this section, DET is considered to demonstrate the role of the proposed method in performance assessment and parameters selection, and to reveal how the coupling effect and the bandlimiting affect the anti-multipath performance of 2-D loops.

1) *Multipath Error Envelope:* For two worst cases in which the multipath is in-phase ($\phi = 0$) and out-of-phase ($\phi = \pi$) with the direct signal, respectively, substituting (25) into (29) and linearizing $\delta_c^m(\tau_c, \tau_s)$ and $\delta_s^m(\tau_c, \tau_s)$ at $[\tau_c^i, \tau_s^i]^T$ yields discriminator slopes

$$\begin{cases} \kappa_{cc}^i = 2 \int_{-\beta_r}^{\beta_r} v(f) \cos(\pi f \Delta_c) \varpi_c^\pm(f) df \\ \kappa_{cs}^i = -2 \int_{-\beta_r}^{\beta_r} v(f) \varpi_s^\pm(f) df \\ \kappa_{sc}^i = -2 \int_{-\beta_r}^{\beta_r} v(f) \varpi_c^\pm(f) df \\ \kappa_{ss}^i = 2 \int_{-\beta_r}^{\beta_r} v(f) \frac{\cos[\pi f (\Delta_s - T_s)]}{\cos(\pi f T_s)} \varpi_s^\pm(f) df \end{cases} \quad (31)$$

where $v(f) \triangleq 2\pi f \eta(f)/\tan(\pi f T_s)$, and $\varpi_j^\pm(f) \triangleq \cos(2\pi f \tau_j^i) \pm \alpha \cos(2\pi f (\tau_j^i + \Delta\tau))$, for $j \in \{c, s\}$. In

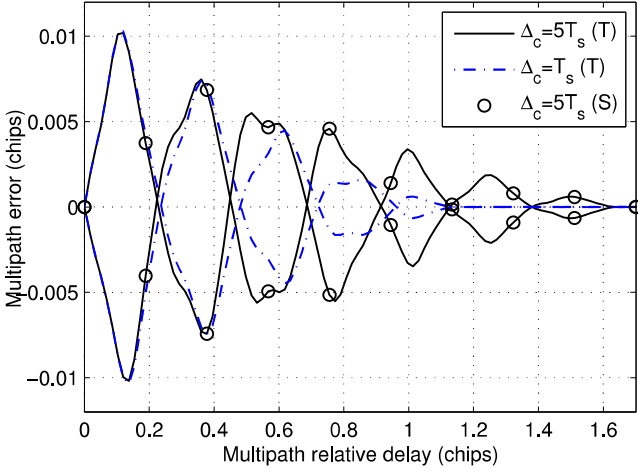


Fig. 9. Theoretical (T) and simulation (S) multipath error envelope of $\text{BOC}_{\sin}(2,1)$ signal for DET.

$\varpi_j^\pm(f)$, the plus and minus signs before α correspond to the in-phase and out-of-phase cases, respectively. Substituting (31) into (28) and using the computational method given in Section V, yields the multipath error envelope.

Fig. 9 shows the results for bandlimited $\text{BOC}_{\sin}(2n, n)$ signals, where α is -10 dB , $\Delta_s = T_s$, and $\beta_r = 12f_c$. Two different code spacings, $\Delta_c = 5T_s$ and $\Delta_c = T_s$, are taken. For comparison, the simulated result for the $\Delta_c = 5T_s$ case, which is obtained via the computer simulation of the baseband tracking process as used in [20], is also plotted in the same figure.

The agreement between the analytical method and the simulation is sufficient to conclude that the theoretical analysis can properly reflect the multipath performance of the 2-D tracking loop. It should be pointed out that the computational burden of obtaining the theoretical result is much less than that of the simulation result. In order to obtain the multipath error envelope, the simulation has to be rerun for each multipath relative delay and relative delay phase. The amount of rerun time is further increased significantly for design parameter iteration, which is time consuming and computationally demanding.

2) *Influence of Coupling Effect:* In Fig. 9, a phenomenon worth noting is that the region suffering the multipath influence is mainly determined by Δ_c . With $\Delta_c = 5T_s$, the maximum multipath delay that can affect the ranging error is approximately $1.6T_c$, while that in the $\Delta_c = T_s$ case is only $1.1T_c$. Without realizing the coupling between the code dimension and the subcarrier dimension, this result is counterintuitive, since in 2-D tracking loops, the final ranging accuracy is mainly determined by the subcarrier loops. And it could be deduced from Fig. 5 that when $\Delta\tau > T_c$, the multipath would no longer affect the subcarrier discriminator so that the 2-D loop would be insensitive to all multipaths whose delays are greater than T_c .

However, note that in (31) both κ_{sc}^i and κ_{cs}^i are nonzero, which implies that the code discriminator and the subcarrier discriminator interact with each other. By using the explicit

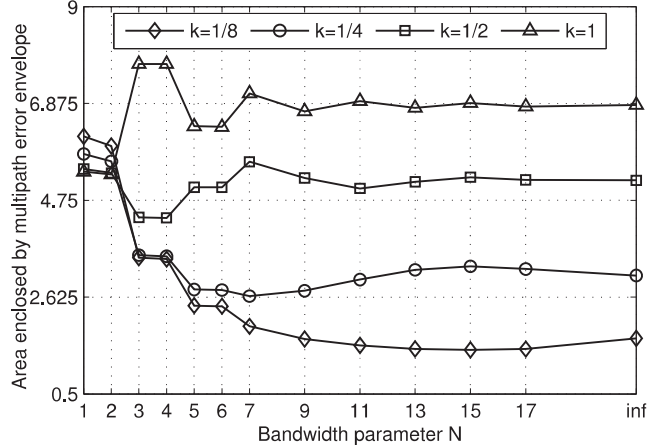


Fig. 10. Area enclosed by the multipath error envelope of $\text{BOC}_{\sin}(2n, n)$ signal by using DET with different subcarrier correlation spacing, $\alpha = -10 \text{ dB}$, $\Delta_c = T_s$, $\Delta_s = kT_s$ for $k = 1, \frac{1}{2}, \frac{1}{4}, \frac{1}{8}$ and $\beta_r = (2N + 1)f_c$ for $N = 1, 2, \dots, 17$, even ∞ .

expression of δ_s , (39), it can be verified that when $\tau_c \neq 0$, the zero-crossing point of the subcarrier discriminator curve will leave the center, which means that tracking errors in the code tracking loop can induce tracking bias in the subcarrier tracking loop. Therefore, when multipath exists, the subcarrier tracking result can be affected by multipath in two ways: the *direct influence* and the *indirect influence*.

The so-called direct influence is that when multipath delay is shorter than the code chip length T_c , as shown in the left part of Fig. 5, the correlation value A_1 and A_2 used for the subcarrier discriminator will be perturbed by multipath, resulting in tracking bias in the subcarrier loop. The so-called indirect influence is that when the multipath delay is in the range of T_c to $T_c + \Delta_c/2$, as the right part of Fig. 5 shows, though the multipath cannot pollute A_1 and A_2 anymore, it can still contaminate B_2 , thus causing code tracking bias. Due to the coupling relation, this code tracking bias can further induce tracking bias in subcarrier loop. The final multipath error is the combination of results from these two different effects. Therefore, in the 2-D loop parameters optimizing for antimultipath performance, both of the discriminators must be fully considered.

3) *Influence of Bandlimiting:* The proposed method can also be used to examine the relationship between discriminator spacing, front-end bandwidths, and the multipath performance, providing guidance to receiver designers in the selection of the optimal design parameters. In Fig. 10, we calculate the area enclosed by the multipath error envelope of $\text{BOC}_{\sin}(2n, n)$ modulated signals, with $\Delta_c = T_s$, α is -10 dB , $\Delta_s = kT_s$ for $k = 1, \frac{1}{2}, \frac{1}{4}, \frac{1}{8}$, and $\beta_r = (2N + 1)f_c$ for $N = 1, 2, \dots, 17, \infty$. From results shown in Fig. 10 it can be observed that when the front-end bandwidth is relative narrow, e.g., $N = 1, 2$, there is no significant difference between error envelope areas with different Δ_s . However, as bandwidth increases, the multipath performance difference that comes from Δ_s becomes more obvious. With a wide front-end bandwidth, a smaller Δ_s results in a better antimultipath performance.

C. Summary

The case studies given in this section, on one hand, reveals the coupling effect and bandlimiting effect on 2-D CCF and its influence on the 2-D tracking. On the other hand, they also show the significance of the proposed theoretical analysis methods in the assessment of performance and the selection of algorithm design parameters. Compared to analysis approaches that simply depend on simulations, theoretical analysis can not only obtain parametric analytical results which are more accurate and universal, but also derive a more clear and essential mechanism interpretation of phenomena.

Since the performance optimization and comparison of specific 2-D tracking techniques are not the focus of this paper, we will not go into it further here. However, it is believed that the proposed exact explicit expressions of 2-D CCF and the general theoretical noise and multipath performances analysis frameworks can be greatly useful in future 2-D tracking technique development.

VII. CONCLUSION AND FUTURE WORK

This paper has presented derivation and extended discussions of a comprehensive description of code-tracking performance for general 2-D loops for BOC signals under conditions where the major error sources are thermal noise and multipath. First, the exact explicit expressions for 2-D correlation functions of BOC signals are proposed. Both the effects of the local subcarrier waveform mismatching and front-end bandlimiting are considered. Based on these exact expressions, the key characteristics of 2-D correlation functions, such as shape, coupling relation between dimensions, and the effects of bandlimiting, are clearly shown. These characteristics are key to assessing the tracking performance of 2-D loops. Second, according to the characteristics of the dimension coupling, general analytical frameworks are provided to analyze the performance of the 2-D tracking techniques under the wireless environment with multipath and noise. The results obtained facilitate investigations in the area of the 2-D tracking technique parameter optimization and performance assessment.

Furthermore, in this paper, the noise and multipath performances of some representative 2-D tracking techniques are provided as specialized application instances of the general results. Important results are obtained for the first time, such as the contributions of the early-late code spacing to both the tracking jitter and the antimultipath performance of subcarrier loop, and the sensitivity of the tracking accuracy and the antimultipath capability to the front-end bandwidth and early-late subcarrier spacing. These case studies, on one hand, reflect the distinctive feature of 2-D tracking compared to 1-D tracking, and, on the other hand, also demonstrate the significance of the proposed theoretical analysis methods in the selection of algorithm design parameters and performance assessment.

Due to space limitations, this paper cannot show more application examples of the proposed theoretical analysis frameworks. However, for future research, performance

comparative studies of different 2-D tracking techniques can be carried out based on the results of this paper. Also, optimal discriminator parameter selection under given bandwidths is recommended for future research. With the proposed canonical 2-D tracking loop model and the 2-D CCF expressions which supports waveform mismatching, designing the optimal 2-D loop-based multipath mitigation technique through the optimization of local subcarrier waveform and discriminator form is also a promising research direction.

APPENDIX A DERIVATION OF $\chi(\tau_c, \tau_s)$

In (8), there is no restriction on the specific value of T , however, it can be assumed that $T \approx lT_c$, where l is a large positive integer. Substituting (3) and $b_{\text{BOC}}(t) = \sum_{n=-\infty}^{\infty} (-1)^n \Pi_{T_s}(t - nT_s)$ into (8), and interchanging the operations of integration and summation, we have

$$\begin{aligned} \chi(\tau_c, \tau_s) &= \frac{1}{lT_c} \sum_{i=-\infty}^{\infty} \sum_{j=-\infty}^{\infty} \sum_{m=-\infty}^{\infty} \sum_{n=-\infty}^{\infty} \\ &\quad \times \int_0^{lT_c} (-1)^m c_i c_j \Pi_{T_c}(t - iT_c) \Pi_{T_c}(t - jT_c - \tau_c) \\ &\quad \times \Pi_{T_s}(t - mT_s) \tilde{q}(t - 2nT_s - \tau_s) dt. \end{aligned} \quad (32)$$

Since $\Pi_{T_c}(t)$ and $\Pi_{T_s}(t)$ are nonzero only when $t \in [0, T_c]$ and $t \in [0, T_s]$, respectively, the integral in (32) is nonzero only when $\Pi_{T_c}(t - iT_c)$, $\Pi_{T_c}(t - jT_c - \tau_c)$ and $\Pi_{T_s}(t - mT_s)$ partially overlap. With the ideal spreading sequence autocorrelation characteristics assumption, we can rewrite (32) into (9), which can be further expanded as

$$\begin{aligned} \chi(\tau_c, \tau_s) &= \frac{1}{T_c} \sum_{n=-\infty}^{\infty} \sum_{m=0}^{2M-1} \int_0^{T_s} (-1)^m \Pi_{T_c}(t + mT_s - \tau_c) \\ &\quad \times \tilde{q}(t - (2n-m)T_s - \tau_s) dt. \end{aligned} \quad (33)$$

For an odd harmonic $\tilde{b}(t)$, $\tilde{q}(t) = \tilde{q}_0(t) - \tilde{q}_0(t - T_s)$, in which $\tilde{q}_0(t)$ is nonzero only when $t \in [0, T_s]$, (33) can be further simplified as

$$\chi(\tau_c, \tau_s) = \frac{1}{T_c} \sum_{m=0}^{M-1} \int_0^{T_s} \Pi_{T_c}(t + mT_s - \tau_c) \Gamma(t; \tau_s) dt \quad (34)$$

where

$$\Gamma(t; \tau_s) \triangleq \sum_{n=-\infty}^{\infty} (-1)^n \tilde{q}_0(t - nT_s - \tau_s). \quad (35)$$

Note that when $\tau_s \in [0, T_s]$, the value of n in (35) can only be 0 or -1 in order to ensure that the part of $\tilde{q}_0(t - 2nT_s - \tau_s)$ within the integral interval is not always zero. Similarly, when $\tau_s \in (-T_s, 0)$, the value of n can only be 0 or 1. Hence, the substantial summation indices in (35) are only $n = 0$ and $n = \pm 1$. So, $\Gamma(t; \tau_s)$ can be rewritten as

$$\Gamma(t; \tau_s) = \tilde{q}_0(t - \tau_s) - \tilde{q}_0(t - \tau_s + T_s \text{sgn}(\tau_s)). \quad (36)$$

Furthermore, note that any τ_c in the interval $(-T_c, T_c)$ can be expressed as $\tau_c = \text{sgn}(\tau_c)[T_c - kT_s - \varepsilon]$, where $k = \lfloor (T_c - |\tau_c|) / T_s \rfloor$, $\varepsilon = T_c - |\tau_c| - kT_s$, and $\varepsilon \in [0, T_s)$. To ensure that $\Pi_{T_c}(t + mT_s - \tau_c)$ and the integral interval in (34) can be overlap partly, when $\tau_c \geq 0$, the value of m must meet $2M - 1 - k \leq m \leq 2M - 1$, which simplifies (34) into

$$\chi(\tau_c, \tau_s) = \frac{k}{T_c} \int_0^{T_s} \Gamma(t; \tau_s) dt + \frac{1}{T_c} \int_0^{\varepsilon} \Gamma(t; \tau_s - T_s) dt. \quad (37)$$

Similarly, when $\tau_c < 0$, the value of m must meet $0 \leq m \leq k$, and in this case (34) can be simplified as

$$\chi(\tau_c, \tau_s) = \frac{k}{T_c} \int_0^{T_s} \Gamma(t; \tau_s) dt + \frac{1}{T_c} \int_0^{\varepsilon} \Gamma(t; \tau_s) dt. \quad (38)$$

Synthesizing (37) and (38), we can get a unified form $\chi(\tau_c, \tau_s)$, which is (12).

B DERIVATION OF K AND N FOR DET AND DPE

Substituting (18) into (29), we can obtain the function of the subcarrier discriminator output of DET with respect to τ_c and τ_s , which is

$$\delta_s(\tau_c, \tau_s) = \int_{-\beta_r}^{\beta_r} \frac{2\eta(f)}{\sin(\pi f T_s)} [\cos[\pi f (\Delta_s - T_s)] \sin(2\pi f \tau_s) - \cos(\pi f T_s) \sin(2\pi f \tau_c)] df. \quad (39)$$

It is interesting to note that τ_c exists in the right-hand side of (39), which implies that the code discriminator results will affect the subcarrier tracking.

For the code discriminator, in order to eliminate $\Lambda(x)$ and $\text{sgn}(\Lambda(x))$ in (18), different early-late spacings Δ_c must be discussed separately. We focus on the cases for which the early-late spacings Δ_c are close to integral multiples of T_s , in which $\Delta_c/2$ can be decomposed into

$$\frac{\Delta_c}{2} \approx k_1 \cdot 2T_s + k_2 T_s + k_0 \frac{T_s}{2} \quad (40)$$

where $k_1 \in \mathbb{N}$, k_2 and k_0 can take only 0 or 1.

It is easy to verify that when Δ_c is close to an odd multiple of T_s , i.e., $k_0 = 1$, the function of the code discriminator output with respect to τ_c and τ_s can be simplified as

$$\delta_c(\tau_c, \tau_s) = 2 \int_{-\beta_r}^{\beta_r} (-1)^{k_2} \eta(f) \left(\frac{\sin(2\pi f \tau_c) \cos(\pi f \Delta_c)}{\tan(\pi f T_s)} - \frac{\cos[\pi f T_s + (-1)^{k_2} 4\pi f (k_2 + k_1) T_s] \sin(2\pi f \tau_s)}{\sin(\pi f T_s)} \right) df. \quad (41)$$

Substituting (39) and (41) into (21), one can obtain the slope matrix, entries of which are

$$\left\{ \begin{array}{l} \kappa_{sc} = -2 \int_{-\beta_r}^{\beta_r} v(f) df \\ \kappa_{ss} = 2 \int_{-\beta_r}^{\beta_r} v(f) \cos[\pi f (\Delta_s - T_s)] / \cos(\pi f T_s) df \\ \kappa_{cc} = 2(-1)^{k_2} \int_{-\beta_r}^{\beta_r} v(f) \cos(\pi f \Delta_c) df \\ \kappa_{cs} = 2(-1)^{k_2+1} \int_{-\beta_r}^{\beta_r} v(f) \\ \times \frac{\cos[\pi f T_s + (-1)^{k_2} 4\pi f (k_1 + k_2) T_s]}{\cos(\pi f T_s)} df \end{array} \right. \quad (42)$$

where $v(f) \triangleq 2\pi f \eta(f) / \tan(\pi f T_s)$.

When Δ_c is close to even multiples of T_s , in which we have $k_0 = 0$, the function of the code discriminator output with respect to τ_c and τ_s can be written as

$$\delta_c(\tau_c, \tau_s) = 2 \int_{-\beta_r}^{\beta_r} (-1)^{k_2} \eta(f) \sin(\pi f \Delta_c) \{ \sin(2\pi f \tau_s) - 2 \sin(\pi f (\tau_c + \tau_s)) \sin(\pi f |\tau_c - \tau_s|) / \tan(\pi f T_s) \} df. \quad (43)$$

It is worth noting that in this case $\partial \delta_c / (\partial \tau_c)|_{\tau_c=0, \tau_s=0} = 0$, which means the code discriminator is insensitive to the code error when both the code error and the subcarrier error are small. Then, we can obtain the slope matrix, entries of which are

$$\left\{ \begin{array}{l} \kappa_{sc} = -2 \int_{-\beta_r}^{\beta_r} v(f) df \\ \kappa_{ss} = 2 \int_{-\beta_r}^{\beta_r} v(f) \cos[\pi f (\Delta_s - T_s)] / \cos(\pi f T_s) df \\ \kappa_{cs} = 4\pi (-1)^{k_2} \int_{-\beta_r}^{\beta_r} f \eta(f) \sin(\pi f \Delta_c) df \\ \kappa_{cc} \approx 0 \end{array} \right. \quad (44)$$

For DPE, the slope matrix can be obtained via a similar process. Due to the continuity of the integrand, entries for DPE case have unified forms

$$\left\{ \begin{array}{l} \kappa'_{cc} = 2 \int_{-\beta_r}^{\beta_r} v(f) \cos(\pi f \Delta_c) \sin(\pi f_{sc} \Delta_c) df \\ \kappa'_{cs} = 2 \int_{-\beta_r}^{\beta_r} v(f) f_{sc} [\cos(\pi f \Delta_c) \sin(\pi f_{sc} \Delta_c) \\ - f \cos(\pi f_{sc} \Delta_c) \sin(\pi f \Delta_c)] / (f^2 - f_{sc}^2) df \\ \kappa'_{sc} = \int_{-\beta_r}^{\beta_r} v(f) df \\ \kappa'_{ss} = \int_{-\beta_r}^{\beta_r} v(f) f_{sc}^2 / (f_{sc}^2 - f^2) df. \end{array} \right. \quad (45)$$

However, when Δ_c is close to even multiples of T_s , κ'_{cc} is also very near zero.

With the normalized signal amplitude, the noise components of DET at the outputs of the correlators can be

modeled as

$$\begin{cases} n_s^- = T^{-1} \int_0^T n(t) \tilde{g}_c(t - \tau_c) \tilde{b}(t - \tau_s - \frac{\Delta_s}{2}) dt \\ n_s^+ = T^{-1} \int_0^T n(t) \tilde{g}_c(t - \tau_c) \tilde{b}(t - \tau_s + \frac{\Delta_s}{2}) dt \\ n_c^- = T^{-1} \int_0^T n(t) \tilde{g}_c(t - \tau_c - \frac{\Delta_c}{2}) \tilde{b}(t - \tau_s) dt \\ n_c^+ = T^{-1} \int_0^T n(t) \tilde{g}_c(t - \tau_c + \frac{\Delta_c}{2}) \tilde{b}(t - \tau_s) dt. \end{cases} \quad (46)$$

They are zero-mean-dependent noise. The variances at the output of the code and subcarrier discriminators are

$$n_{cc} = E \left\{ |n_c^- - n_c^+|^2 \right\} \quad (47)$$

$$n_{ss} = E \left\{ |n_s^- - n_s^+|^2 \right\} \quad (48)$$

respectively. Substituting (46) into (47) and (48), after some trivial simplification, we can obtain

$$\begin{cases} n_{cc} = 2\alpha \int_{-\beta_r}^{\beta_r} \left\{ \Psi_{\Delta_c}^{\Delta_c}(f) - \operatorname{Re} \left\{ \Psi_{\Delta_c}^{-\Delta_c}(f) e^{j2\pi f \Delta_c} \right\} \right\} df \\ n_{ss} = 2\alpha \int_{-\beta_r}^{\beta_r} \left\{ \Psi_{\Delta_s}^{\Delta_s}(f) - \operatorname{Re} \left\{ \Psi_{\Delta_s}^{-\Delta_s}(f) \right\} \right\} df \\ n_{cs} = \alpha \int_{-\beta_r}^{\beta_r} \operatorname{Re} \left\{ \left[\Psi_{\Delta_c}^{\Delta_s}(f) - \Psi_{\Delta_c}^{-\Delta_s}(f) \right] e^{j\pi f \Delta_c} \right. \\ \quad \left. + \left[\Psi_{-\Delta_c}^{-\Delta_s}(f) - \Psi_{-\Delta_c}^{\Delta_s}(f) \right] e^{-j\pi f \Delta_c} \right\} df \end{cases} \quad (49)$$

where $\alpha = (2T \cdot T_c \cdot C/N_0)^{-1}$, and $\Psi_{t_0}^{t_1}(f) \triangleq B_B^{(t_0/2)}(f) B_B^{(t_1/2)*}(f)$. The expressions of entries of N for DPE are

$$\begin{cases} n'_{cc} = \int_{-\beta_r}^{\beta_r} \frac{8\alpha \sin^2(\pi f T_c)}{\pi^2 (f^2 - f_{sc}^2)^2} [f_{sc} \cos(\pi f_{sc} \Delta_c) \sin(\pi f \Delta_c) \\ \quad - f \cos(\pi f \Delta_c) \sin(\pi f_{sc} \Delta_c)]^2 df \\ n'_{cs} = - \int_{-\beta_r}^{\beta_r} \frac{4\alpha \sin^2(\pi f T_c)}{\pi^2 (f^2 - f_{sc}^2)^2} [f_{sc} \cos(\pi f_{sc} \Delta_c) \sin(\pi f \Delta_c) \\ \quad + f \cos(\pi f \Delta_c) \sin(\pi f_{sc} \Delta_c)]^2 df \\ n'_{ss} = \frac{2\alpha}{\pi^2} \int_{-\beta_r}^{\beta_r} \frac{f^2 \sin^2(\pi f T_c)}{(f^2 - f_{sc}^2)^2} df \end{cases} \quad (50)$$

which can be derived by a similar process.

REFERENCES

- [1] J. W. Betz
The offset carrier modulation for GPS modernization
In *Proc. Inst. Navig. GPS Conf.*, 1999, pp. 639–648.
- [2] C. Mongredien, A. Rgamer, M. Overbeck, G. Rohmer, P. Berglez, and E. Wasle
Opportunities and challenges for multi-constellation, multi-Frequency automotive GNSS receivers
In *Microelectronic Systems*. Berlin, Germany: Springer, 2011, pp. 157–170.
- [3] P. Fine and W. Wilson
Tracking algorithm for GPS offset carrier signals
In *Proc. Inst. Navig. Nat. Tech. Meeting*, San Diego, CA, USA, 1999, pp. 671–676.
- [4] A. Burian, E. S. Lohan, and M. Renfors
BPSK-like methods for hybrid-search acquisition of Galileo signals
In *Proc. IEEE Int. Conf. Commun.*, 2006, pp. 5211–5216.
- [5] Z. Yao, X. Cui, M. Lu, and Z. Feng
Pseudo-correlation-function-based unambiguous tracking technique for sine-BOC signals
IEEE Trans. Aerosp. Electron. Syst., vol. 46, no. 4, pp. 1782–1796, Oct. 2010.
- [6] O. Julien, C. Macabiau, M. E. Cannon, and G. Lachapelle
ASPeCT: Unambiguous sine-BOC(n, n) acquisition/tracking technique for navigation applications
IEEE Trans. Aerosp. Electron. Syst., vol. 43, no. 1, pp. 150–162, Jan. 2007.
- [7] M. S. Hodgart and P. D. Blunt
Dual estimate receiver of binary offset carrier modulated signals for global navigation satellite systems
Electron. Lett., vol. 43, no. 16, pp. 877–878, 2007.
- [8] M. S. Hodgart, P. D. Blunt, and M. Unwin
Double estimator a new receiver principle for tracking BOC signals
Inside GNSS, vol. 3, no. 3, pp. 26–36, 2008.
- [9] P. D. Blunt
Advanced global navigation satellite system receiver design
Ph.D. thesis, Univ. Surrey, Guildford, U.K., 2007.
- [10] M. S. Hodgart and E. Simons,
“Improvements and additions to the double estimation technique
In *Proc. IEEE 6th ESA Workshop Satell. Navig. Technol. Eur. Workshop GNSS Signals Signal Process.*, 2012, pp. 1–7.
- [11] P. Blunt, R. Weiler, and M. S. Hodgart
Demonstration of BOC (15, 2.5) acquisition and tracking with a prototype hardware receiver
In *Proc. Eur. Navig. Conf. Eur. Inst. Navig.*, 2007, pp. 1–11.
- [12] J. Ren *et al.*,
“Unambiguous tracking method for alternative binary offset carrier modulated signals based on dual estimate loop
IEEE Commun. Lett., vol. 16, no. 11, pp. 1737–1740, Nov. 2012.
- [13] D. Borio
Double phase estimator: A new unambiguous BOC tracking algorithm
IET Radar Sonar Navig., vol. 8, no. 7, pp. 729–741, Aug. 2014.
- [14] J. Wendel, F. M. Schubert, and S. Hager
A robust technique for unambiguous BOC tracking
In *Proc. 26th Int. Tech. Meeting Satell. Div. Inst. Navig.*, Sep. 2013, pp. 3536–3547.
- [15] T. Feng
Decimation double-phase estimator: An efficient and unambiguous high-order binary offset carrier tracking algorithm
IEEE Signal Process. Lett., vol. 23, no. 7, pp. 905–909, Jul. 2016.
- [16] F. M. Schubert, J. Wendel, M. Sollner, M. Kaindl, and R. Kohl
The astrium correlator: Unambiguous tracking of high-rate BOC signals
In *Proc. IEEE/ION Position, Location Navig. Symp.*, Monterey, CA, USA, May 2014, pp. 589–601.
- [17] J. W. Betz and K. R. Kolodziejki
Generalized theory of code tracking with an early-late discriminator part I: Lower bound and coherent processing
IEEE Trans. Aerosp. Electron. Syst., vol. 45, no. 4, pp. 1538–1550, Oct. 2009.
- [18] D. Borio, P. Anantharamu, and G. Lachapelle
SATLSim: A semi-analytic framework for fast GNSS tracking loop simulations
GPS Solutions, vol. 15, pp. 427–431, 2011.
- [19] I. Markus, J. A. Rodriguez, and G. W. Hein
Criteria for GNSS multipath performance assessment
In *Proc. 18th Int. Tech. Meeting Satell. Div. Inst. Navig.*, 2005, pp. 2166–2177.
- [20] J. M. Kelly, M. S. Braash, and M. F. DiBenedetto
Characterization of the effects of high multipath phase rates in GPS
GPS Solutions, vol. 7, no. 1, pp. 5–15, 2003.



Zheng Yao (S'08–M'10) received the B.Eng. degree in electronics information engineering and the Ph.D. (Hons.) degrees in information and communication engineering from Tsinghua University, Beijing, China, in 2005 and 2010, respectively.

He is currently an Associate Professor in the Department of Electronic Engineering, Tsinghua University. His current research mainly targets next-generation satellite navigation signals design, software-defined receiver, new wireless location technologies, and personal and vehicular positioning in challenging environments.



Yang Gao received the B.Eng. degree in electronic and information engineering and the Ph.D. degree in information and communication engineering from Tsinghua University, Beijing, China, in 2007 and 2014, respectively.

He is currently an Engineer of Beijing Satellite Navigation Center, Beijing. His research interests include satellite positioning and statistical signal processing.



Yang Gao received the B.Eng. degree in electronic information engineering from Tsinghua University, Beijing, China, in 2013. He is currently working toward the Ph.D. degree in the Department of Electronic Engineering, Tsinghua University.

His current research focuses on new generation GNSS signal processing and real-time GNSS software receiver.



Mingquan Lu received the M.E. and Ph.D. degrees in electronic engineering from the University of Electronic Science and Technology of China, Chengdu, China, in 1993 and 1999, respectively.

He is a Professor in the Department of Electronic Engineering, Tsinghua University, Beijing, China. He is the Director of Tsinghua GNSS Research Laboratory, and a member of the Expert Group of China BeiDou Navigation Satellite System. His current research interests include GNSS signal design and analysis, GNSS signal processing and receiver development, GNSS system modeling and simulation, etc.